The Nonuniform Discrete Fourier Transform and Its Applications in Filter Design: Part II—2-D

Sonali Bagchi, *Member, IEEE*, and Sanjit K. Mitra, *Fellow, IEEE*

***Abstract*— The concept of the *nonuniform discrete Fourier transform* (NDFT) is extended to two dimensions to provide a basic framework for nonuniform sampling of 2-D sequences in the frequency domain. The 2-D NDFT of a sequence of size $N_1 \times N_2$ is defined as samples of its 2-D z-transform evaluated at N_1N_2 distinct points located in the 4-D (z_1, z_2) space. These points are chosen appropriately so that the inverse transform exists. We discuss two special cases in which the choice of the sampling points is constrained so that the 2-D NDFT matrix is guaranteed to be nonsingular, and the number of operations required for computing its inverse is reduced. The 2-D NDFT is applied to nonuniform frequency sampling design of 2-D finite-impulse-response (FIR) filters. Nonseparable filters with good passband shapes and low peak ripples are obtained. This is illustrated by design examples, in which 2-D filters with various shapes are designed and compared with those obtained by other existing methods.**

I. Introduction

FOR A SEQUENCE OF LENGTH N, the nonuniform discrete Fourier transform (NDFT), introduced in a companion paper [1], represents samples of its z-transform evaluated at N distinct points located arbitrarily on the z-plane. In this paper, we extend the concept of the NDFT to two dimensions. This provides a basic framework for nonuniform sampling of two-dimensional (2-D) sequences in the frequency domain, which is of interest in many applications. The NDFT of a 2-D sequence corresponds to samples of its 2-D z-transform. The 2-D discrete Fourier transform (DFT) is a special case of the 2-D NDFT, obtained when the sampling points are located on a uniform grid in the 2-D frequency plane.

As an application of the 2-D NDFT, we use it to design 2-D FIR filters by nonuniform frequency sampling. Earlier efforts in nonuniform 2-D frequency sampling design have involved either constrained sampling structures which reduce computational complexity [2]–[6], or a linear least squares approach that guarantees unique interpolation [4]. Although some of these methods are computationally efficient, the design examples presented in papers show that it is often difficult to design 2-D filters with complex passband shapes using constrained sampling structures. Besides, there are no clear guidelines for locating the frequency samples to design a filter with a desired shape and acceptable quality. Our approach to this problem is to use generalized frequency sampling, where the samples are placed on contour lines that match the desired shape of the passband or stopband of the 2-D filter. The proposed method produces nonseparable 2-D filters with good passband shapes and low peak ripples. Filters of good quality are obtained, even with small regions of support. This is important since such filters are most likely to be used in practical filtering applications.

This paper is organized as follows. The 2-D NDFT is defined in Section II. This is followed by a discussion on two special cases of the 2-D NDFT, obtained when the choice of sampling points is constrained. In Section III, we discuss the application of the 2-D NDFT in 2-D FIR filter design. The general strategy for the proposed 2-D nonuniform frequency-sampling filter design method is outlined. Details of the procedure for designing 2-D filters with square, circular, diamond, fan-shaped passbands are then given. We also present filter design examples and comparisons with filters obtained by other design methods.

II. The 2-D NDFT

As in the case of a 1-D sequence [1], the *nonuniform discrete Fourier transform* of a 2-D sequence corresponds to sampling its 2-D z-transform. The 2-D NDFT of a sequence $x[n_1, n_2]$ of size $N_1 \times N_2$ is defined as

$$\hat{X}(z_{1k}, z_{2k}) = \sum_{n_1=0}^{N_1-1} \sum_{n_2=0}^{N_2-1} x[n_1, n_2] z_{1k}^{-n_1} z_{2k}^{-n_2} \qquad k = 0, 1, \cdots, N_1N_2 - 1 \tag{1}$$

where (z_{1k}, z_{2k}) represent N_1N_2 distinct points in the 4-D (z_1, z_2) space. These points can be chosen arbitrarily but such that the inverse transform exists.

We illustrate this by a simple example. Consider the case $N_1 = N_2 = 2$. We can express (1) in a matrix form as

$$\hat{\mathbf{X}} = \mathbf{D}\mathbf{X} \tag{2}$$

Manuscript received December 1, 1994; revised September 5, 1994. This work was supported by University of California MICRO Grants, with matching funds from Tektronix, Inc., Rockwell International Corp., and Digital Instruments, Inc. This paper was recommended by Associate Editor P. A. Regalia.

S. Bagchi was with the Department of Electrical and Computer Engineering, University of California, Santa Barbara, CA 93106 USA. She is now with AT&T Bell Laboratories, Allentown, PA 18103 USA.

S. K. Mitra is with the Department of Electrical and Computer Engineering, University of California, Santa Barbara, CA 93106 USA.

Publisher Item Identifier S 1057-7130(96)03760-3.

where

$$\hat{\mathbf{X}} = \begin{bmatrix} \hat{X}(z_{10}, z_{20}) \\ \hat{X}(z_{11}, z_{21}) \\ \hat{X}(z_{12}, z_{22}) \\ \hat{X}(z_{13}, z_{23}) \end{bmatrix}$$

$$\mathbf{X} = \begin{bmatrix} x[0, 0] \\ x[0, 1] \\ x[1, 0] \\ x[1, 1] \end{bmatrix} \tag{3}$$

and

$$\mathbf{D} = \begin{bmatrix} 1 & z_{20}^{-1} & z_{10}^{-1} & z_{10}^{-1} z_{20}^{-1} \\ 1 & z_{21}^{-1} & z_{11}^{-1} & z_{11}^{-1} z_{21}^{-1} \\ 1 & z_{22}^{-1} & z_{12}^{-1} & z_{12}^{-1} z_{22}^{-1} \\ 1 & z_{23}^{-1} & z_{13}^{-1} & z_{13}^{-1} z_{23}^{-1} \end{bmatrix}. \tag{4}$$

In general, the 2-D NDFT matrix $\mathbf{D}$ is of size $N_1N_2 \times N_1N_2$. It is fully specified by the choice of the N_1N_2 sampling points. For the 2-D NDFT to exist uniquely, these points should be chosen so that $\mathbf{D}$ is nonsingular. In the case of the 1-D NDFT, if the sampling points z_k are distinct, the inverse NDFT is guaranteed to exist uniquely. This occurs because the 1-D NDFT matrix has a determinant that can always be factored as shown in [1]. However, there is no simple extension of this to the 2-D case. Even if the 2-D sampling points are distinct, this does not guarantee the nonsingularity of $\mathbf{D}$. This calls for the need to make a judicious choice of sampling points. Some results have been derived [4] on sufficient conditions under which the equivalent 2-D polynomial interpolation problem has a unique or nonunique solution when the samples are located on irreducible curves. However, no set of necessary and sufficient conditions has been found. This does not pose a serious problem from the point of view of applications. For all practical purposes, we can just perform a check on the determinant of $\mathbf{D}$ to ascertain whether it is nonzero for that particular choice of points. In the general case, the inverse 2-D NDFT is computed by solving a linear system of size N_1N_2, which requires $O(N_1^3N_2^3)$ operations. The computational complexity can be reduced by imposing constraints on the sample locations, as shown in Section II-A.

Note that the definition of the NDFT can be readily extended to higher dimensions.

A. Special Cases of the 2-D NDFT

In general, the determinant of the 2-D NDFT matrix is not factorizable. However, we now consider special cases in which the determinant can be factored. In these cases, the choice of the sampling points is constrained in some manner so that the 2-D NDFT matrix is guaranteed to be nonsingular. This also reduces the number of operations required to compute the inverse 2-D NDFT.

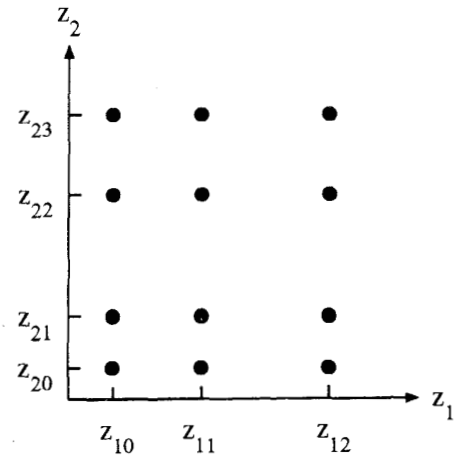

Fig. 1. 2-D NDFT with samples placed at the vertices of a nonuniformly spaced rectangular grid for $N_1 = 3$, $N_2 = 4$.

1) Nonuniformly Spaced Rectangular Grid: In this case, the sampling points lie at the vertices of a rectangular grid in the (z_1, z_2) space. For a sequence of size $N_1 \times N_2$, the z_1-coordinates of the N_1 grid lines running parallel to the z_2 axis can be chosen arbitrarily, provided they are distinct. Let these coordinates be denoted by $z_{10}, z_{11}, \cdots, z_{1,N_1-1}$. Similarly, the z_2-coordinates of the N_2 grid lines running parallel to the z_1 axis can be chosen arbitrarily, provided they are distinct. Let these coordinates be denoted by $z_{20}, z_{21}, \cdots, z_{2,N_2-1}$. This distribution of points is illustrated in Fig. 1, for an example where $N_1 = 3$, $N_2 = 4$. Note that the representation of the z_1 and z_2 axes in this figure is for the sake of illustration only, since the complex variables z_1 and z_2 actually form a 4-D space.

Equation (2) can then be expressed in a simpler matrix form as

$$\hat{\mathbf{X}} = \mathbf{D}_1 \mathbf{X} \mathbf{D}_2^t \tag{5}$$

where (see (6) at the bottom of the page) and

$$\mathbf{X} = \begin{bmatrix} x[0, 0] & x[0, 1] & \cdots & x[0, N_2 - 1] \\ x[1, 0] & x[1, 1] & \cdots & x[1, N_2 - 1] \\ \vdots & \vdots & \ddots & \vdots \\ x[N_1 - 1, 0] & x[N_1 - 1, 1] & \cdots & x[N_1 - 1, N_2 - 1] \end{bmatrix} \tag{7}$$

$$\hat{\mathbf{X}} = \begin{bmatrix} \hat{X}(z_{10}, z_{20}) & \hat{X}(z_{10}, z_{21}) & \cdots & \hat{X}(z_{10}, z_{2,N_2-1}) \\ \hat{X}(z_{11}, z_{20}) & \hat{X}(z_{11}, z_{21}) & \cdots & \hat{X}(z_{11}, z_{2,N_2-1}) \\ \vdots & \vdots & \ddots & \vdots \\ \hat{X}(z_{1,N_1-1}, z_{20}) & \hat{X}(z_{1,N_1-1}, z_{21}) & \cdots & \hat{X}(z_{1,N_1-1}, z_{2,N_2-1}) \end{bmatrix} \tag{6}$$

$$\mathbf{D}_1 = \begin{bmatrix} 1 & z_{10}^{-1} & z_{10}^{-2} & \cdots & z_{10}^{-(N_1-1)} \\ 1 & z_{11}^{-1} & z_{11}^{-2} & \cdots & z_{11}^{-(N_1-1)} \\ \vdots & \vdots & \vdots & \ddots & \vdots \\ 1 & z_{1,N_1-1}^{-1} & z_{1,N_1-1}^{-2} & \cdots & z_{1,N_1-1}^{-(N_1-1)} \end{bmatrix} \tag{8}$$

$$\mathbf{D}_2 = \begin{bmatrix} 1 & z_{20}^{-1} & z_{20}^{-2} & \cdots & z_{20}^{-(N_2-1)} \\ 1 & z_{21}^{-1} & z_{21}^{-2} & \cdots & z_{21}^{-(N_2-1)} \\ \vdots & \vdots & \vdots & \ddots & \vdots \\ 1 & z_{2,N_2-1}^{-1} & z_{2,N_2-1}^{-2} & \cdots & z_{2,N_2-1}^{-(N_2-1)} \end{bmatrix}. \tag{9}$$

Here, $\mathbf{X}$ and $\hat{\mathbf{X}}$ are matrices of size $N_1 \times N_2$. $\mathbf{D}_1$ and $\mathbf{D}_2$ are Vandermonde matrices of sizes $N_1 \times N_1$ and $N_2 \times N_2$, respectively. The equivalent 2-D NDFT matrix $\mathbf{D}$ can be expressed in the form

$$\mathbf{D} = \mathbf{D}_1 \otimes \mathbf{D}_2 \tag{10}$$

where $\otimes$ denotes the Kronecker product [7]. Applying a property of the Kronecker product, the determinant of $\mathbf{D}$ can be written as

$$\begin{aligned} \det(\mathbf{D}) &= \{\det(\mathbf{D}_1)\}^{N_2} \otimes \{\det(\mathbf{D}_2)\}^{N_1} \\ &= \prod_{i \neq j, i>j} (z_{1i}^{-1} - z_{1j}^{-1})^{N_2} \prod_{p \neq q, p>q} (z_{2p}^{-1} - z_{2q}^{-1})^{N_1}. \end{aligned} \tag{11}$$

Therefore, $\mathbf{D}$ is nonsingular provided $\mathbf{D}_1$ and $\mathbf{D}_2$ are nonsingular, i.e., if $z_{10}, z_{11}, \cdots, z_{1,N_1-1}$ are distinct, and $z_{20}, z_{21}, \cdots, z_{2,N_2-1}$ are distinct.

For this choice of sampling points, only $N_1 + N_2$ degrees of freedom are used among the $N_1 N_2$ degrees available in the 2-D NDFT. Consequently, the inverse 2-D NDFT $\mathbf{X}$ in (5) can be computed by solving two separate linear systems of sizes N_1 and N_2, respectively. This involves $O(N_1^3 + N_2^3)$ operations, instead of $O(N_1^3 N_2^3)$ operations in the general case.

A specific case of this sampling structure has been used in [5], where the samples are placed on a nonuniform rectangular grid in the 2-D (ω_1, ω_2) plane ($z_1 = e^{j\omega_1}$, $z_2 = e^{j\omega_2}$). The 2-D DFT is a special case under this category, obtained when the points are chosen on a uniform grid in the (ω_1, ω_2) plane.

2) Nonuniform Sampling on Parallel Lines: This is a generalization of the sampling structure used in Case (1) above. For an $N_1 \times N_2$ sequence, the samples are placed on N_1 lines parallel to the z_2 axis, with N_2 points on each line. The z_1-coordinates corresponding to the N_1 lines can be chosen arbitrarily, but distinct from each other. Let these coordinates be denoted by $z_{10}, z_{11}, \cdots, z_{1,N_1-1}$. Similarly, the z_2-coordinates of the N_2 points on each line can be chosen arbitrarily, provided they are distinct. Let the z_2-coordinates of the points on the ith line be $z_{20i}, z_{21i}, \cdots, z_{2,N_2-1,i}$, where $i = 0, 1, \cdots, N_1 - 1$. Fig. 2 shows an example where $N_1 = 3$, $N_2 = 4$.

In this case, the 2-D NDFT matrix can be expressed as a generalized Kronecker product [7]

$$\mathbf{D} = \{\mathbf{D}_2\} \otimes \mathbf{D}_1. \tag{12}$$

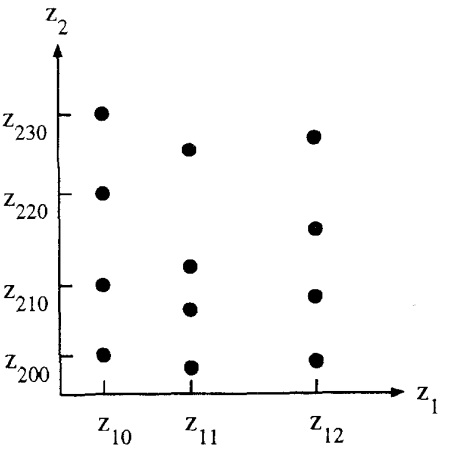

Fig. 2. 2-D NDFT with nonuniform sampling on parallel lines (parallel to the z_2 axis), for $N_1 = 3$, $N_2 = 4$.

Here, $\mathbf{D}_1$ is an $N_1 \times N_1$ Vandermonde matrix as shown in (8). $\{\mathbf{D}_2\}$ denotes a set of N_1 $N_2 \times N_2$ Vandermonde matrices $\mathbf{D}_{2i}$, $i = 0, 1, \cdots, N_1 - 1$. This is represented as

$$\{\mathbf{D}_2\} = \begin{Bmatrix} \mathbf{D}_{20} \\ \mathbf{D}_{21} \\ \vdots \\ \mathbf{D}_{2,N_1-1} \end{Bmatrix} \tag{13}$$

where

$$\mathbf{D}_{2i} = \begin{bmatrix} 1 & z_{20i}^{-1} & z_{20i}^{-2} & \cdots & z_{20i}^{-(N_2-1)} \\ 1 & z_{21i}^{-1} & z_{21i}^{-2} & \cdots & z_{21i}^{-(N_2-1)} \\ \vdots & \vdots & \vdots & \ddots & \vdots \\ 1 & z_{2,N_2-1,i}^{-1} & z_{2,N_2-1,i}^{-2} & \cdots & z_{2,N_2-1,i}^{-(N_2-1)} \end{bmatrix} \quad i = 0, 1, \cdots, N_1 - 1. \tag{14}$$

Equation (12) means that

$$\mathbf{D} = \begin{bmatrix} \mathbf{D}_{20} \otimes \mathbf{d}_0 \\ \mathbf{D}_{21} \otimes \mathbf{d}_1 \\ \vdots \\ \mathbf{D}_{2,N_1-1} \otimes \mathbf{d}_{N_1-1} \end{bmatrix} \tag{15}$$

where $\mathbf{d}_i$ denotes the ith row vector of matrix $\mathbf{D}_1$.

The determinant of $\mathbf{D}$ can then be written as

$$\det(\mathbf{D}) = \{\det(\mathbf{D}_1)\}^{N_2} \prod_{i=0}^{N_1-1} \det(\mathbf{D}_{2i}). \tag{16}$$

Therefore, $\mathbf{D}$ is nonsingular if the matrices $\mathbf{D}_1$ and $\mathbf{D}_{2i}$ are nonsingular. Alternatively, we can also place the samples on N_2 lines parallel to the z_1 axis with N_1 points on each line.

To compute the inverse 2-D NDFT, we have to solve for $x[n_1, n_2]$ from

$$\begin{aligned} \hat{X}(z_{1i}, z_{2ji}) &= \sum_{n_2=0}^{N_2-1} \sum_{n_1=0}^{N_1-1} x[n_1, n_2] z_{1i}^{-n_1} z_{2ji}^{-n_2} \\ &= \sum_{n_2=0}^{N_2-1} y[z_{1i}, n_2] z_{2ji}^{-n_2}, \\ & \qquad i = 0, 1, \cdots, N_1 - 1 \\ & \qquad j = 0, 1, \cdots, N_2 - 1 \end{aligned} \tag{17}$$

where

$$y[z_{1i}, n_2] = \sum_{n_1=0}^{N_1-1} x[n_1, n_2] z_{1i}^{-n_1}. \quad (18)$$

For each value of z_{1i}, $i = 0, 1, \cdots, N_1 - 1$, (17) represents a Vandermonde system of N_2 equations which can be solved to find $y[z_{1i}, n_2]$, $n_2 = 0, 1, \cdots, N_2 - 1$. For each value of n_2, (18) represents a Vandermonde system of N_1 equations which can be solved to obtain $x[n_1, n_2]$, $n_1 = 0, 1, \cdots, N_1 - 1$. Therefore, the inverse 2-D NDFT can be computed by solving N_1 linear systems of size N_2 each, and N_2 linear systems of size N_1 each. This requires $O(N_1 N_2^3 + N_2 N_1^3)$ operations.

A specific case of this sampling structure has been used for 2-D filter design [3], where the samples are placed on parallel lines in the 2-D (ω_1, ω_2) plane. In a recent effort [6], the same structure has been used with a Newton representation for a 2-D filter transfer function. For an $N \times N$ support, the number of operations required to compute the inverse 2-D NDFT is reduced from $O(N^4)$ to $O(N^3)$. Although the sampling structures discussed in Cases 1 and 2 guarantee nonsingularity of the 2-D NDFT matrix, it is difficult to design 2-D filters with complex passband shapes using such constrained sampling.

III. 2-D FIR Filter Design Using the NDFT

We have applied the 2-D NDFT, defined in Section II, to design 2-D FIR filters by nonuniform frequency sampling. Let us first review the existing approaches briefly.

A. Existing Methods for 2-D Frequency Sampling Design

Uniform frequency sampling methods were the first to appear. They involve sampling the 2-D frequency response of the ideal filter at the vertices of a Cartesian grid on the frequency plane, and then solving for the corresponding impulse response using a 2-D inverse DFT [8]. If we use this method to design filters that are piecewise constant, the sharp transition between bands causes large ripples in the resulting frequency response. This is improved considerably if some transition samples are introduced. Computing optimal values for these transition samples requires linear programming methods that minimize the peak ripple [8]. This is computationally intensive due to the large number of constraint equations obtained by sampling the 2-D frequency response over a dense grid. Therefore, this is typically avoided by simply using a reasonable choice for the transition sample values, such as linear interpolation of samples. The inherent disadvantage of uniform frequency sampling is the lack of flexibility in locating the frequency samples. Consequently, the filters deviate from the desired passband shape, especially for small support sizes.

There have been efforts to improve this method by using a *nonuniform* placement of the frequency samples [2]–[6]. The approach proposed by Diamessis *et al.* [2] is based on an extension of Newton interpolation to 2-D. In order to generate a Newton form in 2-D, some topological constraints must be placed on the frequency support. This particular method uses a triangular support for the frequency samples, which makes it difficult to design filters with complex shapes. Angelides [5] has proposed an approach using samples on a nonuniform rectangular grid and a class of 2-D Newton-type polynomials for designing 2-D FIR filters. This reduces the 2-D design problem to two 1-D linear systems, as described in Case 1 of Section II-A. In another method proposed by Rozwood *et al.* [3], the locations of the frequency samples are constrained to be on parallel horizontal or vertical lines in the 2-D frequency plane. As described in Case 2 of Section II-A, this form of sampling reduces the general linear system to smaller sets of equations, thus reducing complexity. Using the same constraints on sampling, Angelides [6] has shown that zero-phase 2-D transfer functions can be represented by Newton polynomials, further reducing the number of operations. These methods provides greater control over passband shapes as compared with uniform frequency sampling, but at the expense of increased ripples. In the two design examples included in [3], some samples were placed along the edges of the passband and stopband to provide control over the shape. However, there is no efficient algorithm which will automatically locate the samples satisfying the constraints, and design a filter of acceptable quality. Zakhor and Alvstad [4] have developed a broader class of nonuniform sampling strategies, in which they constrain the sample locations to be on irreducible curves in the 2-D frequency plane. Their examples of sampling distributions include polar samples, and samples on straight lines. They have derived a theorem that provides conditions for unique interpolation. However, in general, the total number of samples required for unique interpolation exceeds the number of filter coefficients, resulting in a linear least squares solution. A common feature of the designs included in [4] is that a few samples are placed at the intersection of the sampling lines and the edges of the passband and stopband to shape the contours in the desired fashion.

B. Proposed 2-D Nonuniform Frequency Sampling Design

In the proposed 2-D filter design method, the desired frequency response is sampled at N_i points located nonuniformly in the 2-D frequency plane, where N_i is the number of independent filter coefficients. All symmetries present in the filter impulse response are utilized so that N_i is typically much lower than the total number of filter coefficients, N^2. This reduces the design time, besides guaranteeing symmetry. The set of N_i linear equations, given by the 2-D NDFT formulation in (1) is then solved to obtain the filter coefficients.

As in the case of 1-D filter design [1], the choice of sample values and locations depends on the particular type of filter being designed. In general, the problem of locating the 2-D frequency samples is much more complex than in the 1-D case. Our experience in designing 2-D filters with various shapes indicates that best results are obtained when the samples are placed on *contour lines* that match the desired passband shape. For example, to design a square-shaped filter, we place the samples along a set of square contour lines in the 2-D frequency plane. Note that these results agree with the filter design results in [3] and [4], where better control over shape was obtained by placing samples at the edges of the passband and stopband. The total number of contours

and number of samples on each contour have to be chosen carefully so as to avoid singularities. A necessary condition for nonsingularity is known [4, Theorem 2, p. 171], and helps to serve as a rough check. However, this condition is not sufficient to guarantee nonsingularity. The theorem asserts that if the sum of the degrees of the irreducible curves, on which the samples are placed, is small compared to the degree of the filter polynomial, then the interpolation problem becomes singular. Going back to our example of designing a square filter, it is clear that the number of square contours must be chosen appropriately with respect to the filter size.

As we locate the frequency samples along contour lines of the desired shape, the *parameters* to be chosen are: 1) the number of contours and the spacing between them, 2) the number of samples on each contour and their relative spacing, and 3) the sample values. In the following sections, we show how these parameters are chosen for filters with various shapes, such as square, circular, diamond and fan shapes. A common approach used is that a particular *cross-section* of the desired 2-D frequency response is approximated by 1-D analytic functions derived from Chebyshev polynomials, similar to those used for 1-D FIR filter design in [1]. The samples are then placed on contours that pass through the extrema of this cross-section. This will become clear when we look at design examples in the following sections.

C. Square Filter Design

Consider the design of a square-shaped low-pass filter $h[n_1, n_2]$, whose frequency-response specification is shown in Fig. 3. Let the filter be of size $N \times N$, with passband edge ω_p and stopband edge ω_s, as defined in Fig. 3. Since the frequency response exhibits a fourfold symmetry, the zero-phase response $H(\omega_1, \omega_2)$ can be expressed in the form [9]

$$H(\omega_1, \omega_2) = h[0, 0] + \sum_{n_1=1}^{(N-1)/2} 2h[n_1, 0] \cos \omega_1 n_1 + \sum_{n_2=1}^{(N-1)/2} 2h[0, n_2] \cos \omega_2 n_2 + \sum_{n_1=1}^{(N-1)/2} \sum_{n_2=1}^{(N-1)/2} 4h[n_1, n_2] \cdot \cos \omega_1 n_1 \cos \omega_2 n_2. \quad (19)$$

Thus, the number of independent filter coefficients is given by

$$N_i = \frac{(N+1)^2}{4}. \quad (20)$$

To solve for these coefficients, we require N_i samples of $H(\omega_1, \omega_2)$ located in the first quadrant of the (ω_1, ω_2) plane.

Our design method is based on the following idea. If we take a cross-section of the 2-D frequency response along the ω_1 axis (or ω_2 axis), the plot resembles a 1-D low-pass filter response. Given the 2-D filter specifications such as the support size and bandedges, we first represent the passband and stopband of this cross-section by separate analytic functions, $H_p(\omega)$ and $H_s(\omega)$, as was done for 1-D low-pass filter design in [1]. Then we place samples along the ω_1 axis, at the extrema of these functions. In the 2-D frequency plane, the sample locations are on squares passing through these extremal locations. All the samples on a particular square have the same value and are evenly spaced. The total number of square contours is $(N+1)/2$. The number of samples on the kth contour starting from the origin is $(2k-1)$, for $k = 1, 2, \cdots, (N+1)/2$. This choice works well, since the total number of samples is given by the sum of a series of $(N+1)/2$ odd numbers, which equals $(N+1)^2/4$.

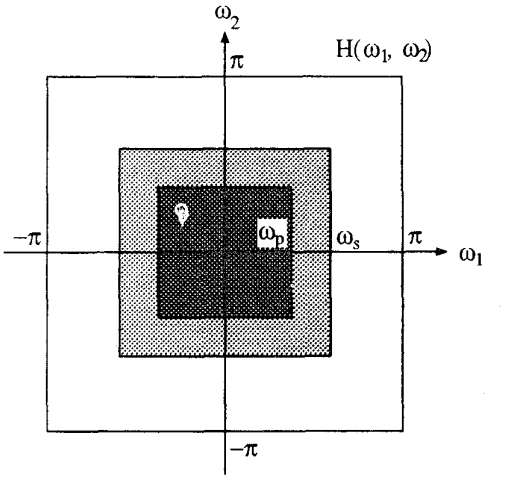

Fig. 3. Frequency-response specification of a square-shaped low-pass filter. Dark region: passband, light region: transition band, unshaded region: stopband.

The filter coefficients are found by solving the N_i equations obtained by sampling (19) at N_i points. The following example illustrates the design method.

Example 1: Consider the design of a square low-pass filter with the specifications: Support size = 9×9, $\omega_p = 0.35\pi$, $\omega_s = 0.65\pi$. Since only 25 of the 81 filter coefficients are independent, we require 25 samples located in the first quadrant of the 2-D frequency plane. The total number of square contours is five. The cross-section of the 2-D frequency response along the ω_1 axis is represented by 1-D analytic functions, as shown in Fig. 4. The location and values of the five samples along the ω_1 axis are obtained by sampling these functions, as denoted by "$*$" in Fig. 4. The remaining samples are placed on five successive squares passing through these points, as illustrated in Fig. 5(b). The frequency response and contour plot of the resulting square filter are shown in Fig. 5(a) and (b). From the contour plot, it is clear that the passband has the desired square shape.

The frequency response of a square filter, shown in Fig. 3, is essentially a separable one. We can design a separable 2-D square filter $h[n_1, n_2]$ by first designing two 1-D low-pass filters $h_1[n]$ and $h_2[n]$, and then simply taking their product along orthogonal directions. Separable filters are widely used in practice because of their design simplicity and ease of

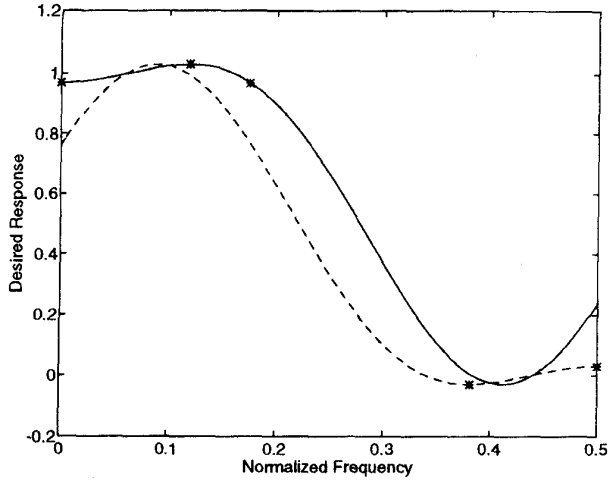

Fig. 4. Generation of analytic functions for square filter designed by the NDFT method. The cross-section of the 2-D frequency response along the ω_1 axis is approximated by $H_p(\omega)$ (solid line) in the passband, and $H_s(\omega)$ (dashed line) in the stopband. These functions are sampled as denoted by "$*$."

TABLE I
PERFORMANCE COMPARISON FOR 2-D FILTERS DESIGNED IN EXAMPLES 1–4

Filter	Method	δ_p	δ_s
Square	NDFT	0.0322	0.0471
	Separable Design	0.1116	0.0579
Circular	NDFT	0.0324	0.0315
	Uniform Sampling	0.0393	0.0519
	Modified Uniform Sampling	0.0245	0.0244
	Nonuniform LLS	0.0360	0.0430
	McClellan Transformation	0.0238	0.0238
	Hazra-Reddy Transformation	0.0587	0.0587
Diamond	NDFT	0.0189	0.0184
	Frequency Transformation	0.0636	0.0636
	Bamberger-Smith	0.1085	0.1084
	Chen-Vaidyanathan	0.0292	0.0281
Fan	NDFT	0.0051	0.0051
	Frequency Transformation	0.0238	0.0238
	Ansari	0.0365	0.0352
	l_p Optimization	0.0223	0.0223

implementation. However, they suffer from the following problem. If δ_{p_1}, δ_{s_1} and δ_{p_2}, δ_{s_2} are the peak ripples in the passband and stopband of the two 1-D filters, respectively, then the resulting 2-D filter can have peak ripples as large as $(\delta_{p_1}+\delta_{p_2})$ in the passband, and $\max(\delta_{s_1}, \delta_{s_2})$ in the stopband. Thus, the 2-D filter might have large passband ripple, which is undesirable. In such cases, much better results can be obtained by utilizing the N^2 degrees of freedom available in designing a nonseparable filter, instead of the $2N$ degrees used in a separable design.

We now compare the nonseparable square filter in Example 1 to a separable filter, designed with the same specifications. The Parks–McClellan algorithm is used to design the corresponding 1-D low-pass filter with length $N = 9$, and bandedges as specified in Example 1. A performance comparison is shown in Table I. We denote the peak ripples obtained in the passband and stopband by δ_p and δ_s, respectively. Note that the peak passband ripple obtained by our method is nearly a third of that present in the separable filter.

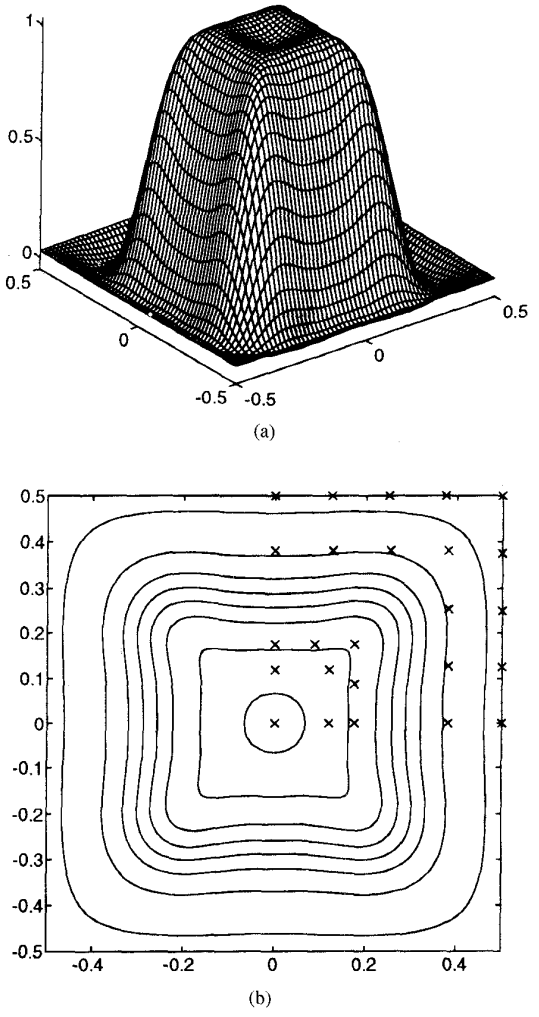

Fig. 5. Square filter of size 9×9 designed by the NDFT method. (a) Plot of frequency response $H(\omega_1, \omega_2)$ with normalized frequencies $(\omega_1/2\pi)$ and $(\omega_2/2\pi)$. (b) Contour plot. The sample locations are denoted by "$\times$."

D. Circularly Symmetric Filter Design

Consider the design of a circularly symmetric low-pass filter of size $N \times N$, which has a frequency-response specification with passband edge ω_p and stopband edge ω_s, as defined in Fig. 6. As for square filter design, we require samples of the desired response at N_i points located in the first quadrant of the frequency plane. These samples are placed on circular contours. Since the cross-section of the 2-D frequency response along the ω_1 axis (or ω_2 axis) resembles a 1-D low-pass response, it is represented by analytic functions as before. The $(N+1)/2$ samples along the ω_1 axis are placed

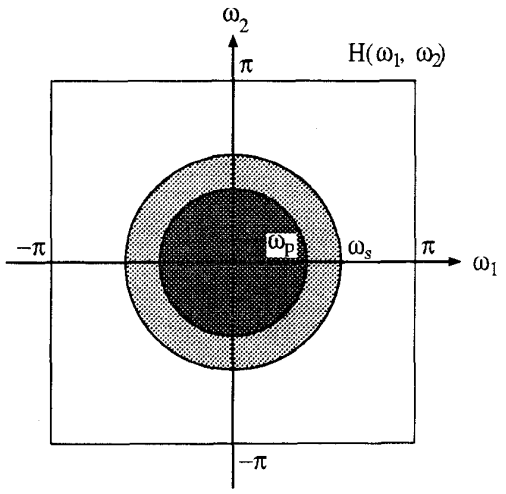

Fig. 6. Frequency-response specification of a circularly symmetric low-pass filter. Dark region: passband, light region: transition band, unshaded region: stopband.

at the extrema of these functions. We can view the process of generating the remaining samples as a rotation of the samples located along the ω_1 axis. For ease of understanding, this is illustrated in Example 2.

Example 2: Consider the design of a circularly symmetric low-pass filter with the specifications: Support size = 15×15, $\omega_p = 0.4\pi$, $\omega_s = 0.6\pi$. The 64 samples required are placed on circular contours, as shown in Fig. 7(b). The values and locations of the eight samples along the ω_1 axis are first obtained by generating the 1-D functions $H_p(\omega)$ and $H_s(\omega)$. These samples are then used to generate 1, 3, 4, 5, 6, 7, 8, 9 samples placed on eight respective circles starting from the origin. The rest of the samples in the upper right corner near (π, π) are placed on circular arcs uniformly spaced from each other. As can be seen in Fig. 7(b), there are 6, 5, 4, 3, 2, 1 samples on six successively smaller arcs. Such a choice of samples works well with a number of other filters designed. For a filter of size $N \times N$, we place $1, 3, 4, 5, \cdots, (N+3)/2$ samples on $(N+1)/2$ circles, and $(N-3)/2, (N-5)/2, \cdots, 3, 2, 1$ samples on $(N-3)/2$ circular arcs, going radially outward from the origin. The samples on a particular circle or arc have the same value and are spaced at equal angles with respect to the origin. Fig. 7(a) and (b) show the frequency response and contour plot of the 15×15 circular low-pass filter. The filter exhibits nearly equiripple characteristics and a high degree of circular symmetry.

For the purpose of comparison, we consider five other methods for circularly symmetric 2-D filter design. These are: 1) uniform frequency sampling [9], 2) modified uniform frequency sampling [10], 3) nonuniform frequency sampling using a linear least squares (LLS) approach [4], 4) the McClellan frequency transformation [11], and 5) the frequency transformation proposed by Hazra and Reddy [12]. We use these methods to design a circular low-pass filter with the specifications used in Example 2, and compare their performances in Table I. Method 1 is the traditional uniform frequency

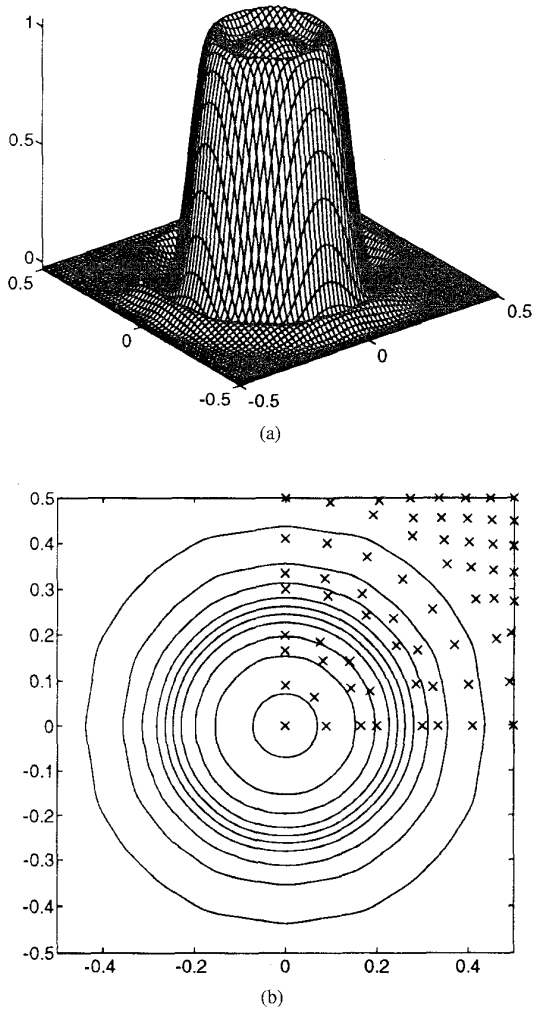

Fig. 7. Circular low-pass filter of size 15×15 designed by the NDFT method. (a) Frequency response. (b) Contour plot. The sample locations are denoted by "×."

sampling technique that uses sample values of unity in the passband and zeros in the stopband. The values of the samples in the transition band are chosen by linear interpolation from zero to unity. It is difficult to control the shape of the passband and stopband contours in this method. In Method 2, the frequency samples are uniformly spaced as in 1. However, the sample values are obtained by uniformly sampling a 2-D analytic function generated by applying the McClellan frequency transformation to the 1-D analytic functions used for 1-D filter design. Methods 2 and 4 produce similar filters, whose contours deviate from the desired circular shape as the frequency increases from 0 to π. In Method 3, nonuniform frequency sampling is used with a least squares approach, as discussed in Section III-A. For comparison, we refer to an example [4, p. 173] that uses the same specifications as in Example 2. The authors note that this method results in contours which are more circular than for uniform frequency sampling in Method 1. Method 5 is an improved frequency transformation technique introduced by Hazra and Reddy. It produces 2-D filters which are much more circular than those

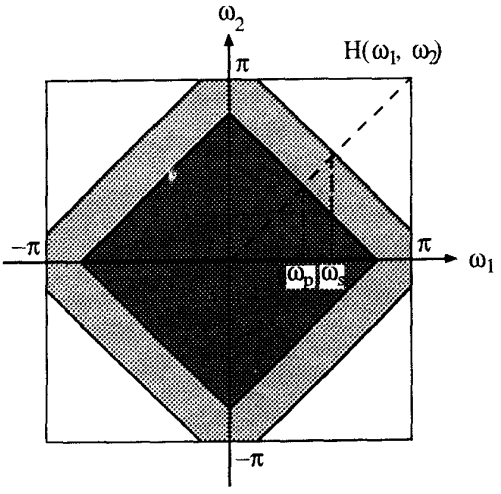

Fig. 8. Frequency-response specification of a diamond filter. Dark region: passband, light region: transition band, unshaded region: stopband.

produced by the McClellan transformation, but at the expense of higher peak ripples for identical filter specifications. For Methods 2 and 4, we have used a transformation of size 3×3. Note that the NDFT method gives a good combination of low peak ripples and circular contour shapes.

E. Diamond and Fan Filter Design

Diamond filters find important practical applications as prefilters for quincunxially sampled data, and in interlaced-to-noninterlaced scanning converters for television signals. A diamond filter has a frequency-response specification with passband edge ω_p and stopband edge ω_s, as shown in Fig. 8. The diagonal line $(\omega_1 = \omega_2)$ in the frequency plane intersects the passband edge at (ω_p, ω_p) and the stopband edge at (ω_s, ω_s). A diamond filter exhibits an eightfold symmetry in the frequency domain [9], and is also a 2-D half-band filter. Its frequency response $H(\omega_1, \omega_2)$ is symmetric about the point $(\omega_1, \omega_2, H) = (\pi/2, \pi/2, 0.5)$ in frequency space. This implies that the impulse response has alternating zeros so that the nonzero coefficients form a quincunx-like lattice. Thus, we get

$$h[n_1, n_2] = \begin{cases} 0, & n_1 + n_2 = \text{even}, \\ 0.5, & n_1 = n_2 = 0. \end{cases} \tag{21}$$

On account of these symmetries, the number of independent coefficients [13] in a filter of size $N \times N$ is reduced to

$$N_i = \left\lfloor \frac{P+1}{2} \right\rfloor \left\lfloor \frac{P+2}{2} \right\rfloor \tag{22}$$

where

$$P = \frac{N-1}{2}. \tag{23}$$

The N_i independent points in the impulse response lie in a wedge-shaped region below the diagonal $(n_1 = n_2)$ in the first quadrant of the (n_1, n_2) spatial plane. Thus, the frequency response of a diamond filter [13] can be expressed as

$$\begin{aligned} H(\omega_1, \omega_2) = 0.5 &+ \sum_{n_1=1}^{\lfloor (P+1)/2 \rfloor} 2h[2n_1 - 1, 0] \\ &\cdot \{\cos(2n_1 - 1)\omega_1 + \cos(2n_1 - 1)\omega_2\} \\ &+ \sum_{n_1=1}^{\lfloor (P+1)/2 \rfloor} \sum_{n_2=1}^{\lfloor P/2 \rfloor} 4h[2n_1 - 1, 2n_2] \\ &\cdot \{\cos(2n_1 - 1)\omega_1 \cos(2n_2)\omega_2 \\ &+ \cos(2n_2)\omega_1 \cos(2n_1 - 1)\omega_2\}. \end{aligned} \tag{24}$$

TABLE II
DISTRIBUTION OF SAMPLES FOR DIAMOND FILTER DESIGN. THE LAST COLUMN SHOWS THE NUMBER OF SAMPLES PLACED ON $(N-1)/2$ SUCCESSIVE CONTOURS FOR DESIGNING A FILTER OF SIZE $N \times N$, WHICH HAS N_i INDEPENDENT COEFFICIENTS

N	N_i	Number of samples on successive contours
7	4	1, 2, 1
9	6	1, 1, 2, 2
11	9	1, 1, 2, 3, 2
13	12	1, 1, 2, 3, 3, 2
15	16	1, 1, 2, 3, 3, 4, 2
17	20	1, 1, 2, 3, 3, 4, 4, 2
19	25	1, 1, 2, 3, 3, 4, 4, 4, 3
21	30	1, 1, 2, 3, 3, 3, 4, 4, 5, 4
23	36	1, 1, 2, 3, 3, 3, 4, 4, 5, 6, 4
25	42	1, 1, 2, 3, 3, 4, 4, 4, 5, 6, 6, 5
27	49	1, 1, 2, 3, 3, 4, 4, 4, 5, 6, 6, 6, 5
29	56	1, 1, 2, 3, 3, 4, 4, 4, 5, 6, 6, 6, 7, 5
31	64	1, 1, 2, 3, 3, 4, 4, 4, 5, 6, 6, 6, 7, 7, 6

Due to the eightfold symmetry and the half-band nature of the filter, the only independent part of the frequency response is a triangular area within the passband, whose vertices are (0, 0), $(\pi, 0)$, $(\pi/2, \pi/2)$. In our design method, N_i samples are placed within this region of the frequency plane. If we take a cross-section of $H(\omega_1, \omega_2)$ along the diagonal line $(\omega_1 = \omega_2)$, it resembles a 1-D half-band low-pass response. We approximate the passband of this response by a 1-D function $H_p(\omega)$, as used for 1-D half-band low-pass filter design in [1]. The order P of the corresponding Chebyshev polynomial $T_P(x)$ is $(N-1)/2$. The samples are then placed on $(N-1)/2$ lines of slope -1, that pass through the extrema of $H_p(\omega)$. All samples on a particular line have the same value and are evenly spaced. The number of samples on successive lines, as we go away from the origin, is given in Table II, for filter sizes from 7×7 to 31×31. This range of filter sizes is large enough to cover the needs of most practical applications. The given distribution of samples has been found to work well for various choices of the bandedges. Note that if there is only one sample to be placed on a particular line, it is placed on the ω_1 axis. Finally, the N_i samples are used to solve for the impulse response coefficients in (24).

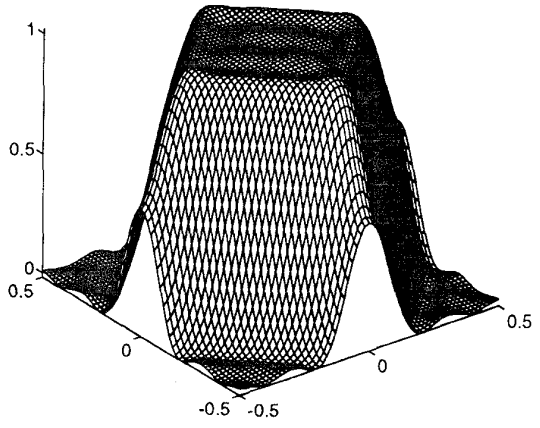

(a)

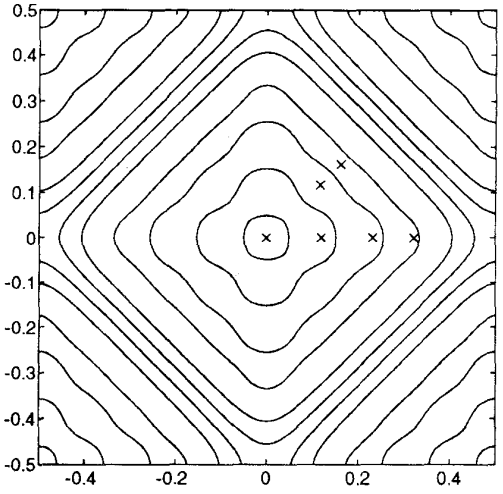

(b)

Fig. 9. Diamond filter of size 9 × 9 designed by the NDFT method. (a) Frequency response. (b) Contour plot. The sample locations are denoted by "×."

The proposed design method produces diamond filters of high quality, with low peak ripple and better passband shape as compared to filters produced by other existing design methods. A comparison between these methods is presented in the following example.

Example 3: Consider the design of a diamond filter with the following specifications: Support size = 9 × 9, $\omega_p = 0.36\pi$, $\omega_s = 0.64\pi$. Only six of the 81 filter coefficients are independent. Thus, six samples are placed as shown in Fig. 9(b), on lines that follow the diamond shape. The diagonal cross-section of the 2-D frequency response is represented by a function $H_p(\omega)$, that has four extrema. Samples are placed on four lines passing through these extrema. The number of samples on these lines are 1, 1, 2, 2, respectively, as given in Table I. Fig. 9(a) and (b) show the frequency response and contour plot of the resulting diamond filter.

For comparison, we now consider three existing methods for designing diamond filters: 1) frequency transformation [9], 2) the method proposed by Bamberger and Smith [14], and 3) the method proposed by Chen and Vaidyanathan [15]. We use each of these methods to design a diamond filter with the same specifications as given in Example 3. A performance comparison is shown in Table I. In Method 1, a low-pass 1-D filter (of length 9) is transformed to a 2-D diamond filter using a 3×3 transformation. This produces contours which are more circular rather than diamond-shaped. The shape of the contours can be improved by using a higher order transformation, but this also increases the filter size considerably. In this example, if we use a 5×5 transformation and the same 1-D filter of length 9, then the 2-D filter size becomes 17×17. So this is uneconomical. In Method 2, a diamond filter is designed by rotating a checkerboard-shaped filter [14] through an angle of 45 degrees. Although the shape of the contours is better than for frequency transformation, the ripple is too large. Method 3 produces a diamond filter with a good passband shape but higher peak ripple, compared with our method. From Table I, we can see that the NDFT method gives the lowest peak ripple among these methods as well as good contour shapes.

Finally, we note that the method proposed for diamond filter design can also be used to design *fan filters*. Fan filters possess directional sensitivity, which is important in applications such as the processing of geoseismic data. A 90-degree fan filter can be obtained by shifting the diamond frequency response by π along the ω_2 axis. Thus, if $(\omega_{1k}, \omega_{2k}, H_k)$ is a sample location for the corresponding diamond filter, then $(\omega_{1k}, \pi - \omega_{2k}, H_k)$ is the sample location to be used for designing the fan filter. Alternatively, if $h_d[n_1, n_2]$ is the impulse response of a diamond filter, we can obtain the corresponding fan filter by taking the fan impulse response to be

$$h[n_1, n_2] = (-1)^{n_2} h_d[n_1, n_2]. \tag{25}$$

In the following example, we design a fan filter using our method, and compare the results with those obtained by three other design methods.

Example 4: Consider the design of a fan filter with the specifications: Support size = 17×17, $\omega_p = 0.43\pi$, $\omega_s = 0.57\pi$. Only 20 of the 289 filter coefficients are independent. The frequency response of the fan filter designed is shown in Fig. 10(a). The sample locations used are shown superimposed on the contour plot in Fig. 10(b). These figures show that a desirable fan shape is obtained along with low peak ripple.

We compare the above filter to three other filters designed with the same specifications, using the methods: 1) frequency transformation [9], 2) Ansari's method [16], and 3) the iterative l_p optimization technique proposed by Lodge and Fahmy [17]. The peak ripples obtained are shown in Table I. As shown here, the NDFT method gives the lowest peak ripple. Besides, the shapes of the contours obtained are much better than with the other methods. In Method 1, we transform a 1-D half-band low-pass filter to a 2-D fan filter by applying the 3×3 transformation $\cos \omega = \frac{1}{2} \cos \omega_1 - \frac{1}{2} \cos \omega_2$. The contours tend to be circular, which is undesirable. In Ansari's method, a 1-D half-band low-pass filter of length 17 is used as a prototype. This filter is used to obtain a 2-D filter that has a passband in the second and fourth quadrants, and a stopband

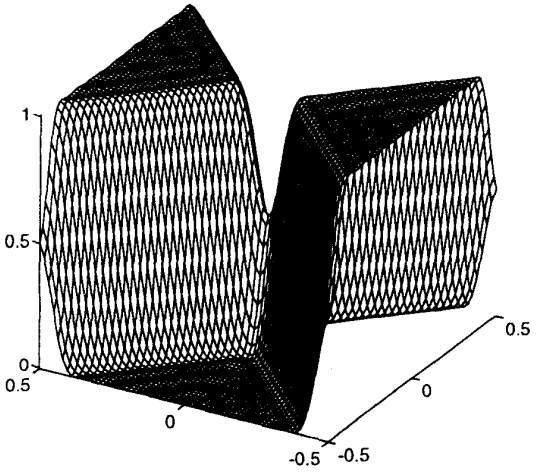

(a)

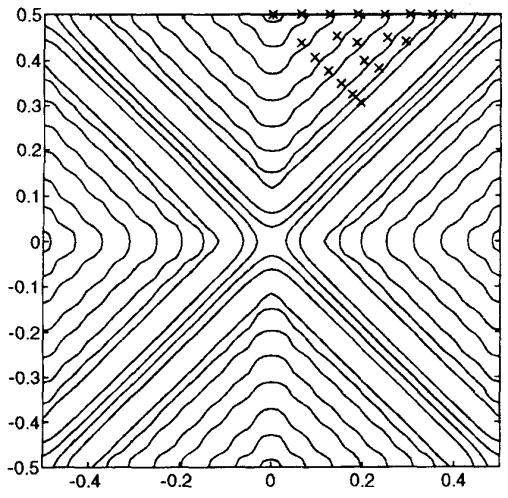

(b)

Fig. 10. Fan filter of size 17 × 17 designed by the NDFT method. (a) Frequency response. (b) Contour plot. The sample locations are denoted by "×."

in the first and third quadrants of the frequency plane. This 2-D filter is then transformed to the desired fan filter by a 45-degree rotation in frequency. Though the shape of the passband is better than in frequency transformation, the peak ripple is also larger. For Method (3), we refer to an example presented by Lodge *et al.* [18, Ex. 1, p. 800], where a fan filter was designed with the same specifications as in Example 4. The contours tend to become circular near $(\pi, 0)$ and $(0, \pi)$.

IV. Conclusion

The concept of the nonuniform discrete Fourier transform was extended to two dimensions in this paper. The 2-D NDFT of a sequence corresponds to samples of its 2-D z-transform. The sequence can be computed from these samples by solving for the inverse 2-D NDFT. This requires a judicious choice of sampling points since no set of necessary and sufficient conditions has yet been found to guarantee a unique solution. We examined two special cases where the samples are constrained so as to reduce computational complexity. In these cases, the 2-D NDFT matrix has a factorizable determinant, and, therefore, can be guaranteed to be nonsingular. The 2-D NDFT was used to develop a nonuniform frequency sampling technique for designing 2-D FIR filters. This method utilizes the freedom of locating samples nonuniformly in the frequency plane to produce nonseparable 2-D filters with good passband shapes and low peak ripple. We demonstrated the design of 2-D filters with a variety of passband shapes, and compared our results with other existing design methods. Earlier nonuniform frequency sampling design methods did not lay down clear guidelines for the choice of sample values and locations. The results are significant owing to the lack of a practical, reliable algorithm to design optimal 2-D filters. We have also investigated the performances of the square-and diamond-shaped filters designed by applying them to schemes for rectangular and quincunx downsampling of images, respectively, [19]. The 2-D filters are used as prefilters prior to downsampling, and as postfilters for interpolating zero-valued samples after upsampling of images. Considering the general problem of nonuniform frequency sampling, we laid down some specific guidelines regarding the choice of the sample values and locations, which were lacking in earlier techniques. These guidelines can serve as a basis for the design of more complex 2-D filters. Finally, the proposed method can be extended to multidimensions for designing 3-D filters which are used for filtering video signals.

References

[1] S. Bagchi and S. K. Mitra, "The nonuniform discrete Fourier transform and its applications in filter design: I—1-D," this issue, pp. 422-433.
[2] J. E. Diamessis, C. W. Therrien, and W. J. Rozwood, "Design of 2–D FIR filters with nonuniform frequency samples," in *Proc. IEEE Int. Conf. Acoust., Speech, Signal Processing,* Dallas, TX, Apr. 1987, vol. 3, pp. 1665–1668.
[3] W. J. Rozwood, C. W. Therrien, and J. S. Lim, "Design of 2-D FIR filters by nonuniform frequency sampling," *IEEE Trans. Acoust., Speech, Signal Processing,* vol. 39, pp. 2508–2514, Nov. 1991.
[4] A. Zakhor and G. Alvstad, "Two-dimensional polynomial interpolation from nonuniform samples," *IEEE Trans. Acoust., Speech, Signal Processing,* vol. 40, pp. 169–180, Jan. 1992.
[5] E. Angelides, "A novel method for modeling 2-D FIR digital filters in frequency domain with nonuniform samples," *IEEE Trans. Circuits Syst. II,* vol. 41, pp. 482–486, July 1994.
[6] ——, "A recursive frequency-sampling method for designing zero-phase FIR filters by nonuniform samples," *IEEE Trans. Signal Processing,* vol. 6, pp. 1461–1467, June 1995.
[7] P. A. Regalia and S. K. Mitra, "Kronecker products, unitary matrices, and signal processing applications," *SIAM Rev.,* vol. 31, pp. 586–613, Dec. 1989.
[8] J. V. Hu and L. R. Rabiner, "Design techniques for two-dimensional digital filters," *IEEE Trans. Audio Electroacoust.,* vol. AU-20, pp. 249–257, Oct. 1972.
[9] J. S. Lim, *Two-Dimensional Signal and Image Processing.* Englewood Cliffs, NJ: Prentice-Hall, 1990.
[10] M. Lightstone, S. K. Mitra, I.-S. Lin, S. Bagchi, P. Jarske, and Y. Neuvo, "Efficient frequency-sampling design of one-and two-dimensional FIR filters using structural subband decomposition," *IEEE Trans. Circuits Syst. II,* vol. 41, pp. 189–201, Mar. 1994.
[11] J. H. McClellan, "The design of two-dimensional digital filters by transformation," in *Proc. 7th Ann. Princeton Conf. Inform. Sci. Syst.,* Princeton, NJ, Mar. 1973, pp. 247–251.
[12] S. N. Hazra and M. S. Reddy, "Design of circularly symmetric low-pass two-dimensional FIR digital filters using transformation," *IEEE Trans. Circuits Syst.,* vol. CAS-33, pp. 1022–1026, Oct. 1986.

[13] T. Yoshida, A. Nishihara, and N. Fujii, "A design method of 2-D maximally flat diamond-shaped half-band FIR filters," *Trans. IEICE (The Inst. Electron., Inform. Commun. Eng.)*, vol. E 73, pp. 901–907, June 1990.
[14] R. H. Bamberger and M. J. T. Smith, "A filter bank for the directional decomposition of images: Theory and design," *IEEE Trans. Signal Processing*, vol. 40, pp. 882–893, Apr. 1992.
[15] T. Chen and P. P. Vaidyanathan, "Multidimensional multirate filters and filter banks derived from one-dimensional filters," *IEEE Trans. Signal Processing*, vol. 41, pp. 1749–1765, May 1993.
[16] R. Ansari and M. S. Reddy, "Efficient IIR and FIR fan filters," *IEEE Trans. Circuits Syst.*, vol. CAS-34, pp. 941–945, Aug. 1987.
[17] J. Lodge and M. M. Fahmy, "An efficient l_p optimization technique for the design of two-dimensional linear-phase FIR digital filters," *IEEE Trans. Acoust., Speech, Signal Processing*, vol. ASSP-28, pp. 308–313, June 1980.
[18] S. A. H. Aly and M. M. Fahmy, "Symmetry in two-dimensional rectangularly sampled digital filters," *IEEE Trans. Acoust., Speech, Signal Processing*, vol. ASSP-29, pp. 794–805, Aug. 1981.
[19] S. Bagchi, "The nonuniform discrete Fourier transform and its applications in signal processing," Ph.D. dissertation, University of California, Santa Barbara, 1994.

Sonali Bagchi (S'90-M'95) for a photograph and biography, see this issue, p. 433.

Sanjit K. Mitra (SM'69-F'74) for a photograph and biography, see this issue, p. 433.